

Supporting information

for

Efficient alkaline water splitting catalyzed by ultrafine Rhodium telluride nanoparticles

Shuyuan Pan^a, Chaofeng Chang^a, Fang Luo^b and Zehui Yang^{a*}

^aSustainable Energy Laboratory, Faculty of Materials Science and Chemistry, China University of Geosciences Wuhan, 388 Lumo RD, Wuhan, 430074, P. R. China.

^bCollege of Materials Science and Engineering, State Key Laboratory of New Textile Materials & Advanced Processing Technology, Wuhan Textile University, Wuhan, 430200, P. R. China.

Experimental section

Materials and chemicals: Rhodium chloride trihydrate ($\text{RhCl}_3 \cdot 3\text{H}_2\text{O}$), Sodium tellurite (Na_2TeO_3), Sodium hydroxide (NaOH), Carbon black (Vulcan XC-72), Nafion solution (5 wt%).

Synthesis of RhTe_2/C : 0.1 mg XC-72 was added into a 250 mL round bottom flask and dispersed in 100 mL ethylene glycol by ultrasound for 30 min. 28.4 mg $\text{RhCl}_3 \cdot 3\text{H}_2\text{O}$ and 43.2 mg Na_2TeO_3 were added and stirred for 30 min. Then the pH was adjusted to 9 with 0.1 M NaOH solution. The device was then set up in an oil bath, reacted at 160 °C for 12 h. Vacuum drying overnight to obtain RhTe_2/C . Rh/C was synthesized by the same method without adding Na_2TeO_3 as contrast sample.

Fundamental characterization: Bruker (D8 Focus) was used for XRD test. The XPS images were collected by Escalab 250Xi (Thermo Scientific). TG curves were measured by STA 409 PC. The TEM images were acquired by JEOL JEM 2100F. TG were obtained by STA 409 PC.

Electrochemical measurement: In electrochemical testing, glassy carbon electrode (GCE), graphitic rod and Hg/HgO were utilized as work, counter and reference electrodes, respectively. The electrolyte was the 1.0 M KOH filled with N_2 (HER)/ O_2 (OER). The polarization curves were measured at the sweep of 5 mV/s. The electrochemical active area was characterized by recording the cyclic voltammetry curves at different sweep speeds, the voltage range was 0.16-0.26 V vs. RHE (HER) and 1.00-1.10 V vs. RHE (OER), respectively. The chronoamperometric test and electrochemical impedance spectroscopy were recorded at a potential of 10 mA cm^{-2} . Cyclic voltammetry was used to cycle between -0.20 and 0.20 V vs. RHE (HER) (1.3-1.7 V vs. RHE (OER)) at the sweep of 100 mV/s, and the polarization curves before and after the cycle were compared to characterize the durability.

Theoretical calculation: All calculations were realized with the Vienna Ab-initio Simulation Package (VASP). Perdew-Burke-Ernzerhof functional was used to describe the exchange related interactions between electrons. We adopted the projector-augmented wave (PAW) pseudopotentials to represent the effect of their ionic cores. The energy cutoff for the plane-wave expansion was set as 500 eV. For the convergence criterion, the atomic force on each atom is less than 0.01 eV/Å, and the energy convergence is better than 10^{-5} eV. The reciprocal sampling of Brillouin zone is generated by VASPKIT. The K points was set as 2 * 2 * 1 for structural optimization, and 3 * 3 * 1 for the density of states calculation.

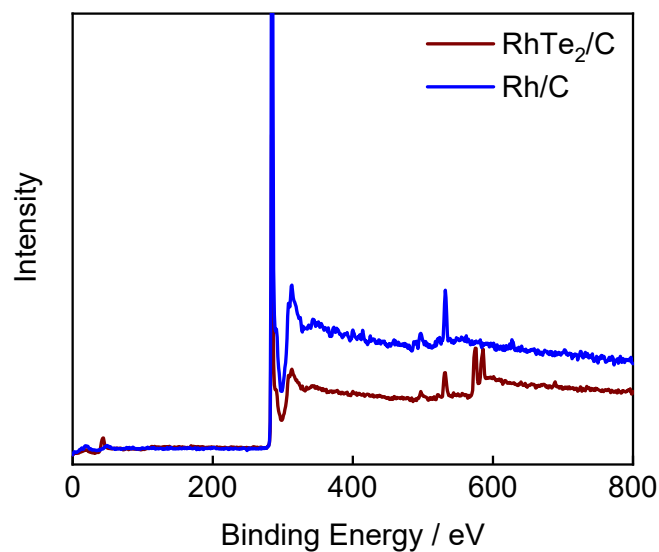


Figure S1 XPS survey scan of Rh/C and RhTe₂/C electrocatalysts.

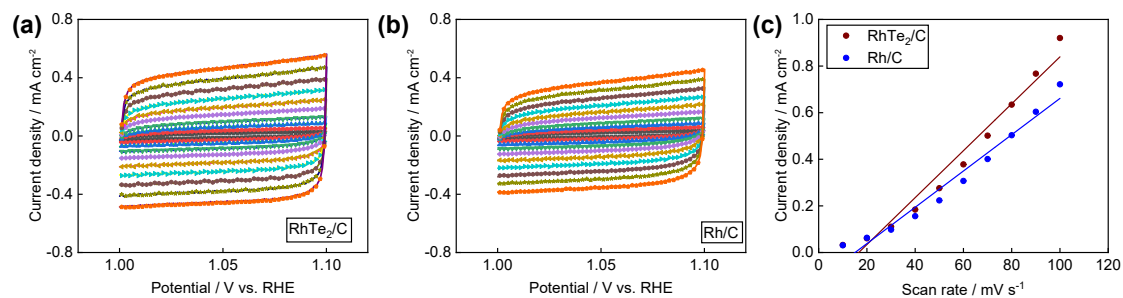


Figure S2 Cyclic voltammetry curves of RhTe₂/C (a) and Rh/C (b). (c) Double layer capacitance of RhTe₂/C and Rh/C in OER catalysis.

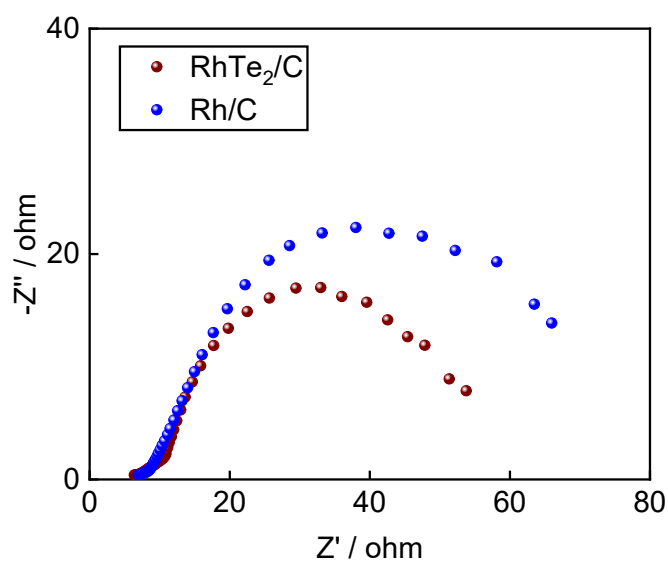


Figure S3 Electrochemical impedance spectroscopies of RhTe₂/C and Rh/C.

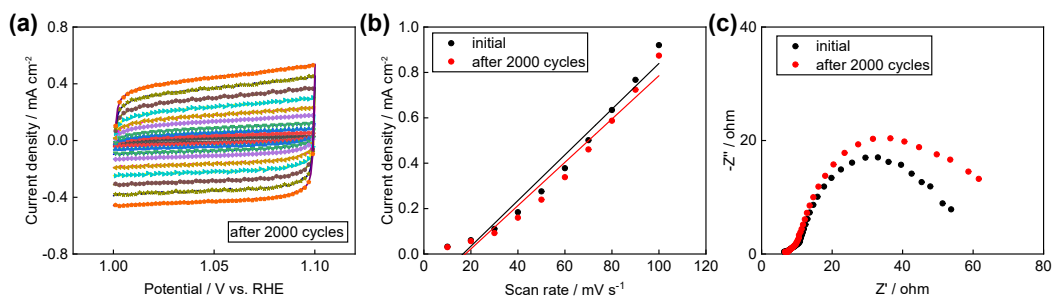


Figure S4 Cyclic voltammety curve (a), double layer capacitance (b) and electrochemical impedance spectroscopies (c) of RhTe₂/C after 2000 cycles.

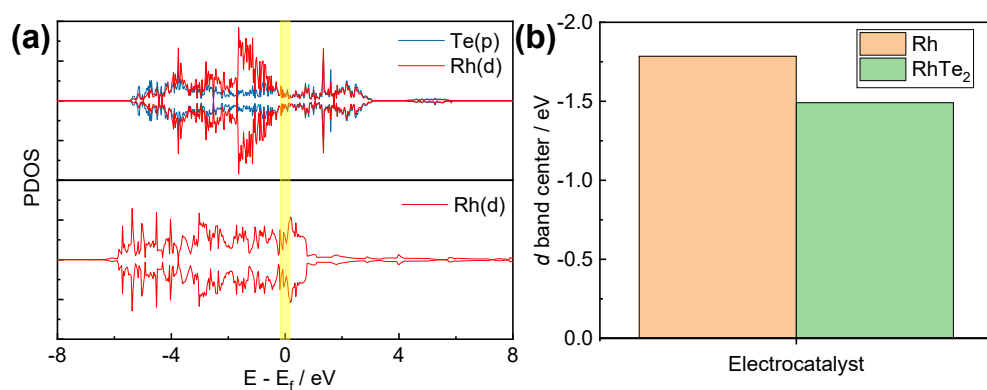


Figure S5 PDOS (a) and *d* band center (b) of Rh and RhTe₂.

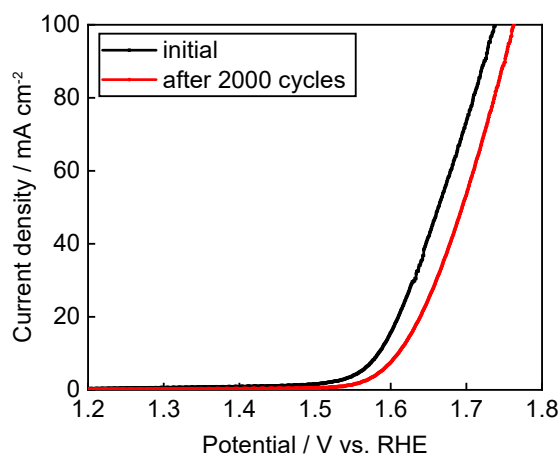


Figure S6 OER performance of Rh/C before and after 2000 cycles.

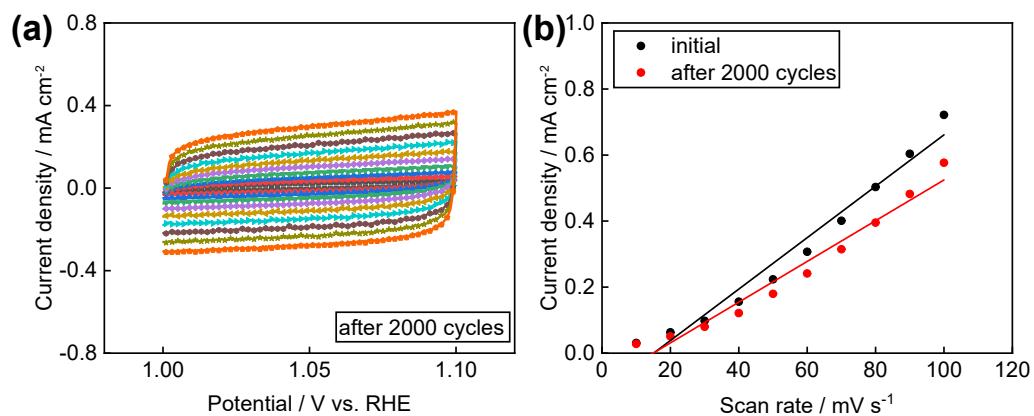


Figure S7 Cyclic voltammery curve (a) and double layer capacitance (b) of Rh/C after 2000 cycles.

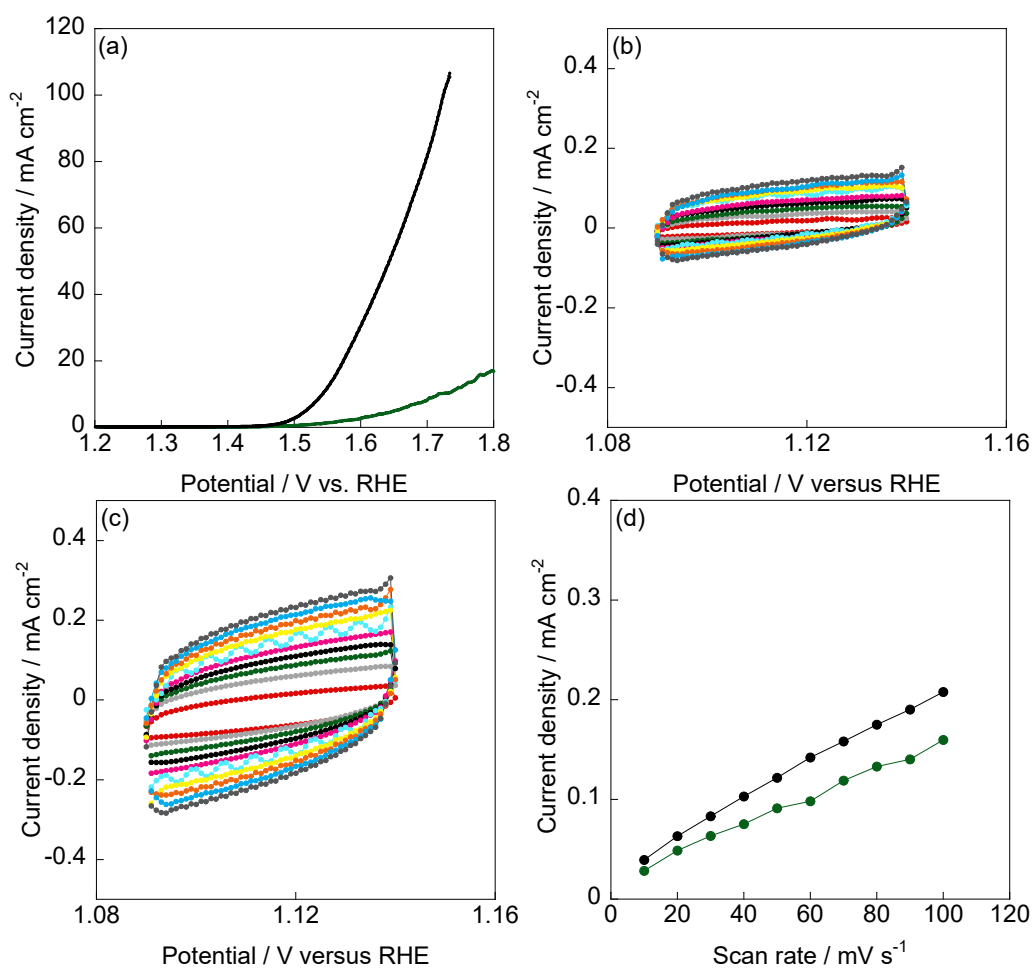


Figure S8 OER performance (a), cyclic voltammery curves (b, c) and double layer capacitance (d) of commercial IrO₂.

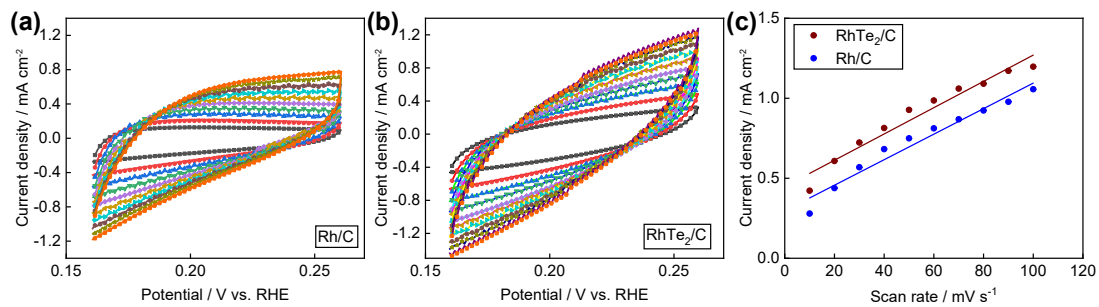


Figure S9 Cyclic voltammograms of RhTe₂/C (a) and Rh/C (b). (c) Double layer capacitance of RhTe₂/C and Rh/C in HER catalysis.

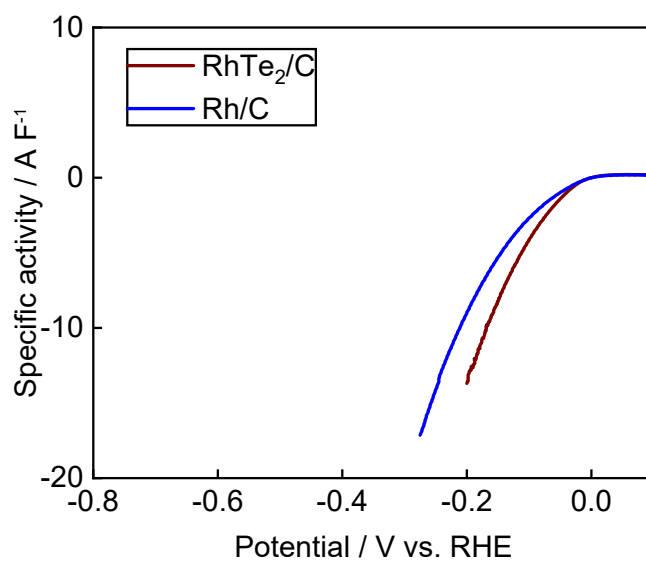


Figure S10 Specific activities of RhTe₂/C and Rh/C in HER catalysis.

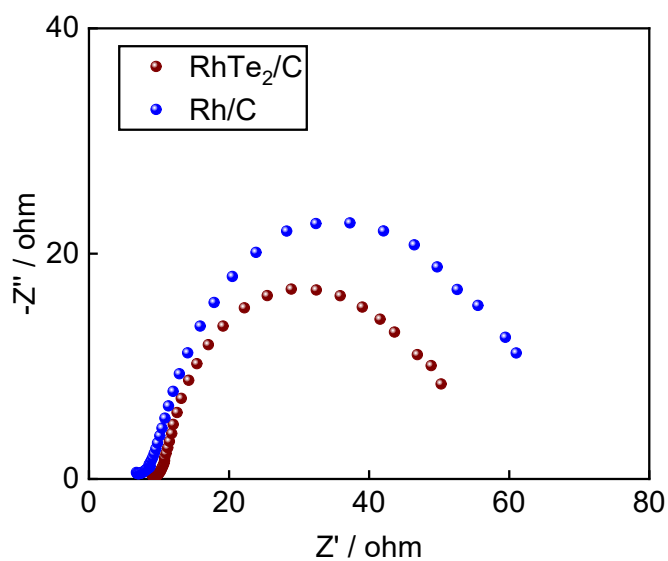


Figure S11 Electrochemical impedance spectroscopies of RhTe₂/C and Rh/C.

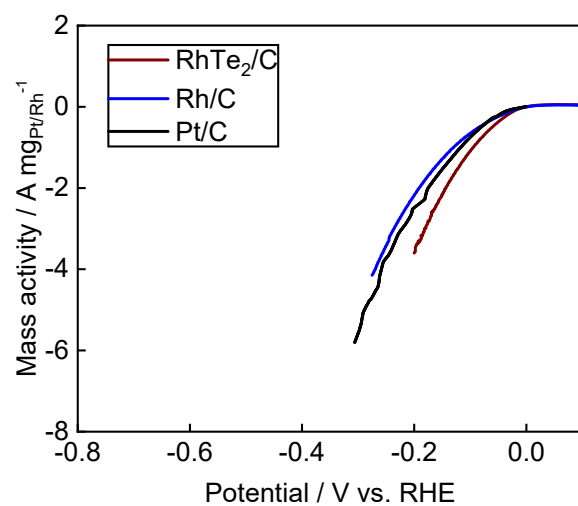


Figure S12 Mass activities of RhTe₂/C, Rh/C and Pt/C in HER catalysis.

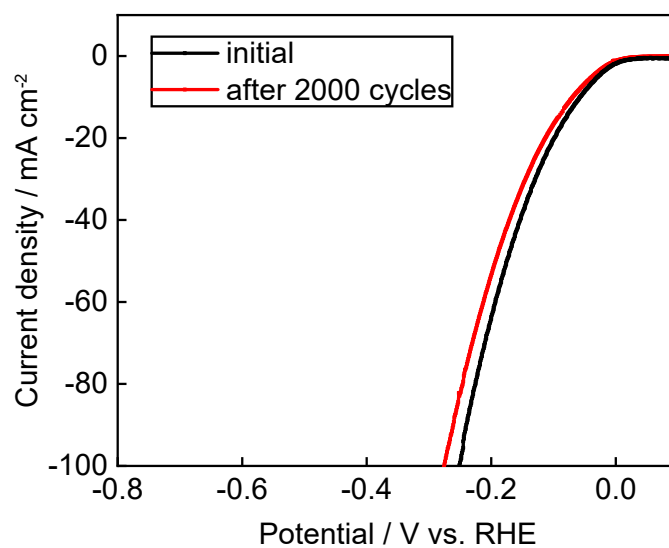


Figure S13 HER stability test of Rh/C before and after 2000 cycles.

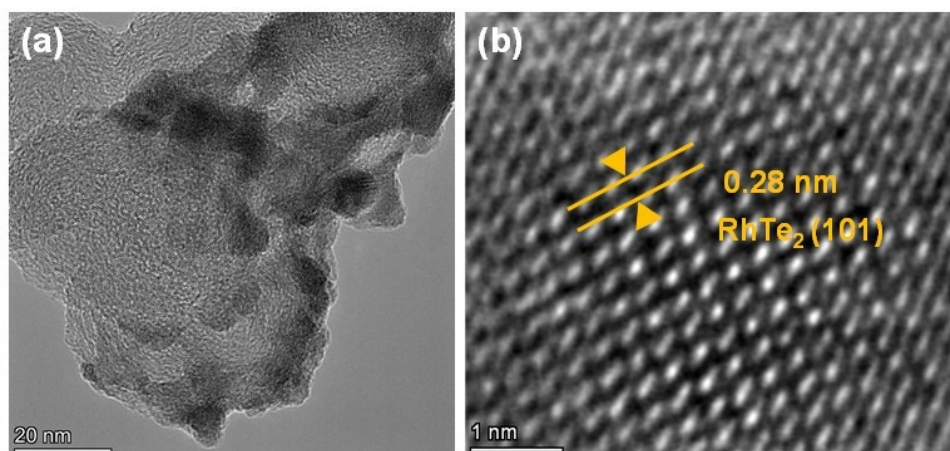


Figure S14 TEM image and HR-TEM image of RhTe₂/C after 2000 cycles.

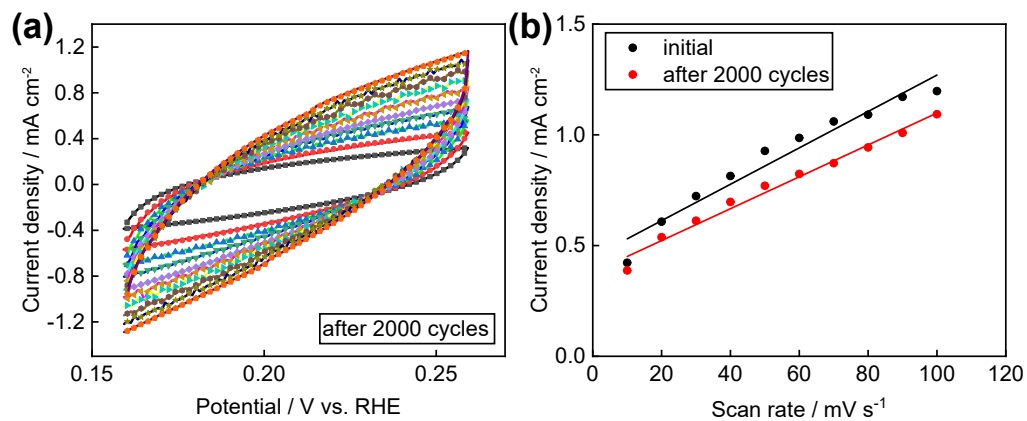


Figure S15 Cyclic voltammetry curve (a) and double layer capacitance (b) of RhTe₂/C after 2000 cycles.

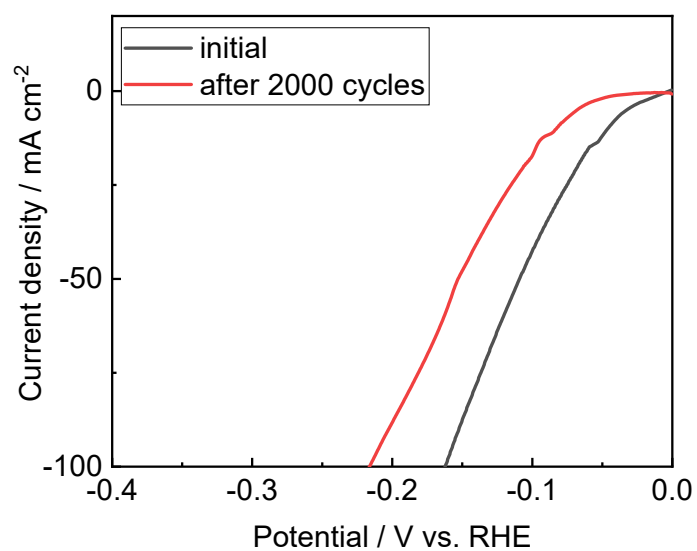


Figure S16 HER stability of commercial Pt/C in HER catalysis.

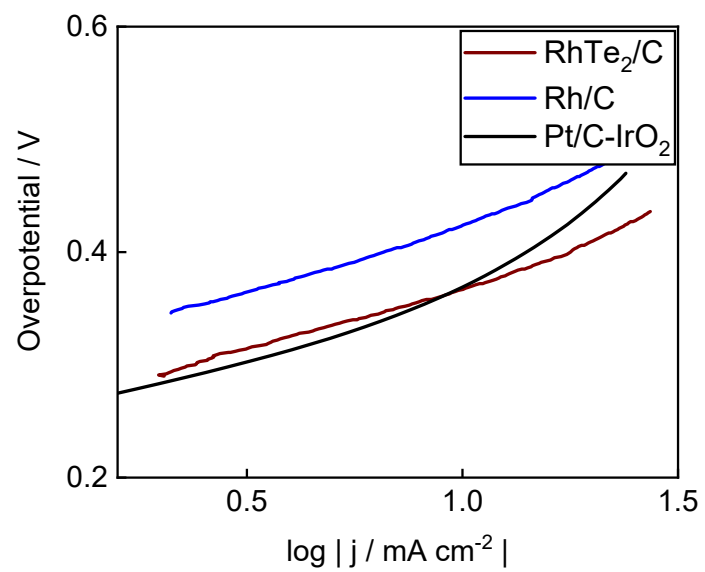


Figure S17 Tafel slopes of RhTe₂/C, Rh/C and Pt/C-IrO₂.